

WASP-41 b: A transiting hot Jupiter planet orbiting a magnetically-active G8 V star

P.F.L. Maxted¹, D.R. Anderson¹, A. Collier Cameron², C. Hellier¹, D. Queloz³, B. Smalley¹, R. A. Street⁴, A.H.M.J. Triaud³, R.G. West⁵, M. Gillon⁶, T.A. Lister⁴, F. Pepe³, D. Pollacco⁷, D. Ségransan³, A. M. S. Smith¹, S. Udry³

ABSTRACT

We report the discovery of a transiting planet with an orbital period of 3.05 d orbiting the star TYC 7247-587-1. The star, WASP-41, is a moderately bright G8 V star ($V=11.6$) with a metallicity close to solar ($[Fe/H] = -0.08 \pm 0.09$). The star shows evidence of moderate chromospheric activity, both from emission in the cores of the Ca II H and K lines and photometric variability with a period of 18.4 d and an amplitude of about 1%. We use a new method to show quantitatively that this periodic signal has a low false alarm probability. The rotation period of the star implies a gyrochronological age for WASP-41 of 1.8 Gyr with an error of about 15%. We have used a combined analysis of the available photometric and spectroscopic data to derive the mass and radius of the planet ($0.92 \pm 0.06 M_{Jup}$, $1.20 \pm 0.06 R_{Jup}$). Further observations of WASP-41 can be used to explore the connections between the properties of hot Jupiter planets and the level of chromospheric activity in their host stars.

Subject headings: Extrasolar planets

1. Introduction

There is continued interest in finding bright stars that host transiting exoplanets because they can be accurately characterized and studied in some detail, e.g., the mass and radius of the planet can be accurately measured. This gives us the opportunity to explore the relationships between the properties of the planet and its host star, e.g., the

orbital eccentricity, the composition and spectral type of the star, the age of the system, etc. Given the wide variety of transiting planets being discovered and the large number of parameters that characterise them, statistical studies will require a large sample of systems to identify and quantify the relationships between these parameters. These relationships can be used to test models of the formation, structure and evolution of short period exoplanets.

Here we report the discovery by the WASP survey of a planetary mass companion to the star TYC 7247-587-1. We find that the star is a G8 V star showing moderate chromospheric activity. The planet, WASP-41 b, is a typical hot Jupiter planet with an orbital period of 3.05 d.

2. Observations

The WASP survey is described in Pollacco et al. (2006) and Wilson et al. (2008) while a discussion of our candidate selection methods can be found in Collier Cameron et al. (2007), Pollacco et al.

¹Astrophysics Group, Keele University, Staffordshire, ST5 5BG, UK

²SUPA, School of Physics and Astronomy, University of St. Andrews, North Haugh, Fife, KY16 9SS, UK

³Observatoire astronomique de l'Université de Genève 51 ch. des Maillettes, 1290 Sauverny, Switzerland

⁴Las Cumbres Observatory, 6740 Cortona Dr. Suite 102, Santa Barbara, CA 93117, USA

⁵Department of Physics and Astronomy, University of Leicester, Leicester, LE1 7RH, UK

⁶Institut d'Astrophysique et de Géophysique, Université de Liège, Allée du 6 Août, 17, Bat. B5C, Liège 1, Belgium,

⁷Astrophysics Research Centre, School of Mathematics & Physics, Queen's University, University Road, Belfast, BT7 1NN, UK

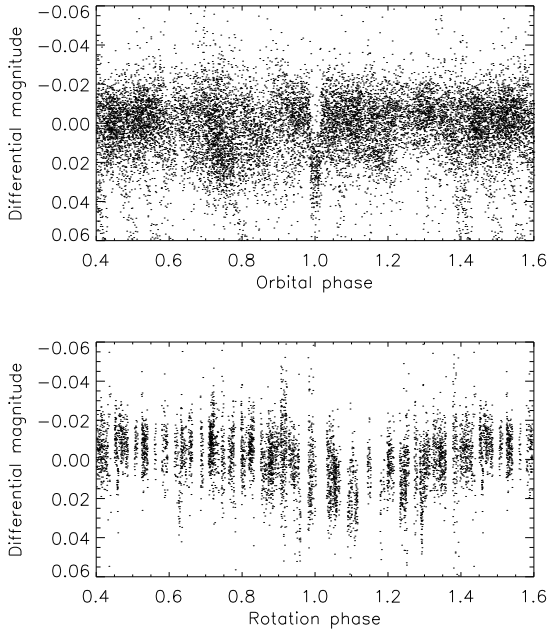


Fig. 1.— WASP-South photometry of WASP-41. Raw data are plotted using small points, phase-binned data are plotted using filled circles. Upper panel: all data plotted as a function of the orbital phase with period $P = 3.0524$ d. Lower panel: data from 2008 plotted as a function of the rotation phase with period $P_{\text{rot}} = 18.4$ d.

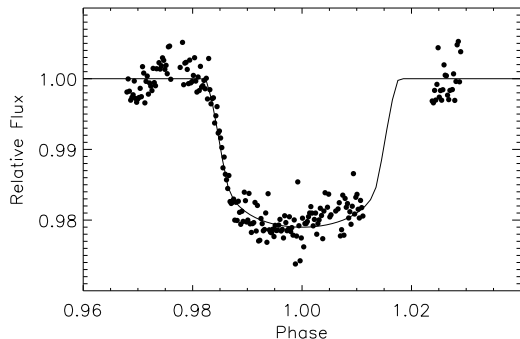


Fig. 2.— Faulkes Telescope South z-band photometry of WASP-41 (points) with the model fit described in Section 5 (solid line).

(2008), and references therein.

The star TYC 7247-587-1 (WASP-41, 1SWASP J124228.50–303823.5) was observed 6767 times by one camera on the WASP-South instrument from 2007 January 20 to 2007 June 22. A further 5637 observations were obtained with the same camera from 2008 January 17 to 2008 May 28.

The WASP-South lightcurves of WASP-41 show transit-like features with a depth of approximately 0.02 magnitudes recurring with a 3.05-d period (Fig. 1). These were independently detected in the WASP-South photometry from the two seasons using the de-trending and transit detection methods described in Collier Cameron et al. (2007), which was taken as good evidence that the periodic transit signal was real. The spectral type of the star was estimated to be approximately G8 based on the catalogue photometry available for this star at the time. The duration and depth of the transit is consistent with the hypothesis that it is due to the transit of a planet-like companion to a main-sequence G8 star and the WASP-South lightcurves show no indication of any ellipsoidal variation due to the distortion of the star by a massive companion.

We obtained 22 radial velocity measurements during the interval 2010 January 3 to 2010 August 5 with the fibre-fed CORALIE spectrograph on the Euler 1.2-m telescope located at La Silla, Chile. The spectra were obtained with an exposure time of 30 minutes and have a typical signal-to-noise ratio of 25–30. Accurate wavelength calibration is ensured by the simultaneous observation of a thorium-argon arc in a second fibre feed to the spectrograph. Details of the instrument and data reduction can be found in Queloz et al. (2000) and references therein. The RV measurements were performed using cross-correlation against a numerical mask generated from a G2-type star and are given in Table 1, where we also provide the bisector span, BS, which measures the asymmetry of the cross-correlation function (Queloz et al. 2001). The standard error of the bisector span measurements is $2\sigma_{\text{RV}}$.

We also obtained photometry of TYC 7247-587-1 and other nearby stars on 2010 June 23 using the LCOGT 2.0-m Faulkes Telescope South (FTS) at Siding Spring Observatory. The Merope camera we used has an image scale of 0.279 arcseconds/pixel when used in the 2x2 binning mode we

employed. We used a Pan-STARRS¹ z-band filter to obtain 210 images covering one transit. These images were processed in the standard way with IRAF² using a stacked bias image, dark frame, and sky flat. The DAOPHOT photometry package (Stetson 1987) was used to perform object detection and aperture photometry for WASP-41 and several comparison stars in the $5' \times 5'$ field of view of the instrument. Observations were interrupted by poor weather so there are no observations during the egress phase of the transit. These data are sufficient to confirm that the transit-like features seen in the WASP-South data are due to the star TYC 7247-587-1 and to provide better measurements of the depth of the transit than is possible from the WASP-South data (Fig. 2).

All photometric data presented in this paper are available from the NStED database.³

3. WASP-41 Stellar Parameters

The 17 individual CORALIE spectra of WASP-41 available up to May 2010 were co-added to produce a single spectrum with a signal-to-noise ratio $\approx 70:1$. The standard pipeline reduction products were used in the analysis.

The analysis was performed using the methods given in Gillon et al. (2009). The H_α line was used to determine the effective temperature (T_{eff}), while the Na I D and Mg I b lines were used as surface gravity ($\log g$) diagnostics. The parameters obtained from the analysis are listed in Table 2. The elemental abundances were determined from equivalent width measurements of several clean and unblended lines. A value for micro-turbulence (ξ_t) was determined from Fe I using the method of Magain (1984). The quoted error estimates include that given by the uncertainties in T_{eff} , $\log g$ and ξ_t , as well as the scatter due to measurement and atomic data uncertainties.

The projected stellar rotation velocity ($v \sin i$) was determined by fitting the profiles of several unblended Fe I lines. A value for macro-turbulence (v_{mac}) of $2.3 \pm 0.3 \text{ km s}^{-1}$ was assumed, based on

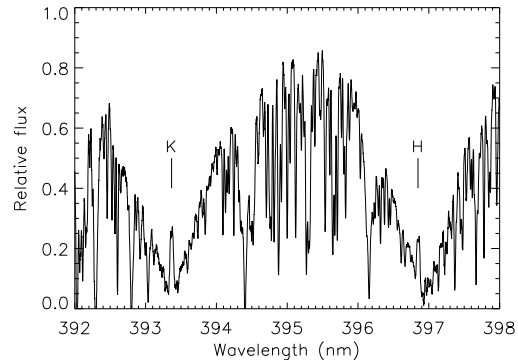


Fig. 3.— Section of the co-added CORALIE spectra of WASP-41 showing emission in the core of the Ca II H and K lines.

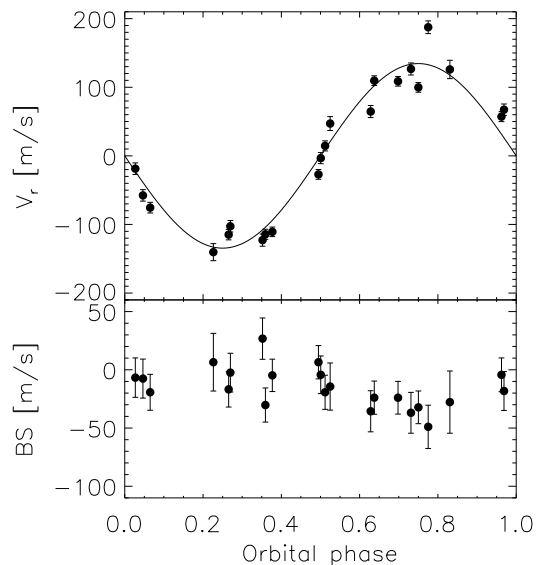


Fig. 5.— Radial velocity and bisector span measurements for WASP-41. Upper panel: Radial velocity relative to the centre-of-mass velocity together with the best-fit circular orbit. Lower panel: bisector span measurements.

¹<http://pan-starrs.ifa.hawaii.edu/public/design-features/camera.html>

²IRAF is distributed by the National Optical Astronomy Observatory, which is operated by the Association of Universities for Research in Astronomy (AURA) under cooperative agreement with the National Science Foundation.

³<http://nsted.ipac.caltech.edu>

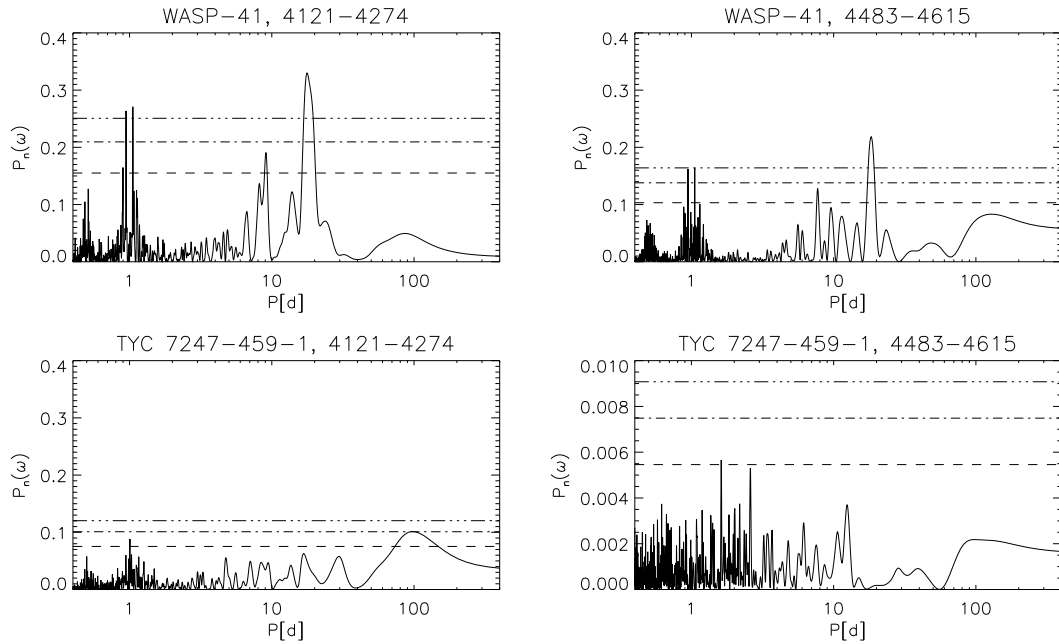


Fig. 4.— Periodogram of the WASP data from two seasons for WASP-41 and TYC 7247-459-1. The star name and date range (JD–245000) are given in the title of each panel. Horizontal lines indicate false alarm probability levels $FAP=0.1,0.01,0.001$. Note the change of scale in the lower right panel.

the tabulation by Gray (2008), and an instrumental FWHM of $0.11 \pm 0.01 \text{ \AA}$, determined from the telluric lines around 6300 \AA . A best fitting value of $v \sin i = 1.6 \pm 1.1 \text{ km s}^{-1}$ was obtained.

We observe emission lines in the cores of the CaII H and K lines in our spectrum of WASP-41 (Fig. 3). We estimate a spectral index $\log R'_{HK} \approx -4.67$ from this spectrum (Noyes et al. 1984), but note that a transformation for measurements made with the CORALIE spectrograph to a standard system does not yet exist.

4. Rotation period

The presence of CaII H and K emission lines in the spectrum of WASP-41 suggests the possibility of variations in the lightcurve due to star spots with the same period as the rotation period of the star. The projected equatorial rotation velocity of WASP-41 combined with the estimated radius given in Table 2 imply a rotation period of $32 \pm 23 \text{ d}$. We therefore searched for photometric variations in our WASP photometry with a similar period.

Our WASP photometry has a large number of observations (several thousand) with standard errors that vary from a few milli-magnitudes for the best data up to a magnitude for data obtained on cloudy nights. WASP data obtained on cloudy nights is sometimes affected by large systematic errors, so we remove data with standard errors larger than 5 times the median value prior to further analysis. The remaining data still have a range of standard errors so it is advantageous to use a period searching algorithm that can account for this. The generalized Lomb-Scargle periodogram defined by Zechmeister and Kürster (2009) is a suitable method. However, there is little to be gained from including a “floating mean” in the case of the WASP data, so we used a slightly different definition of the periodogram equivalent to a least-squares fit of the sinusoidal function $y_i = a \sin(\omega t_i) + b \cos(\omega t_i)$ to magnitudes $m_i = 1, 2, \dots, N$ with standard errors σ_i obtained at times t_i for a given angular frequency ω . Note that we implicitly assume that the magnitudes m_i have a weighted mean value of 0. We used the fol-

Table 1: Radial velocity measurements for WASP-41

BJD	RV	σ_{RV}	BS
-2 450 000	(km s ⁻¹)	(km s ⁻¹)	(km s ⁻¹)
5200.8101	3.1691	0.0076	-0.0168
5290.8090	3.3837	0.0070	-0.0323
5293.8035	3.4106	0.0087	-0.0369
5294.8225	3.2084	0.0077	-0.0193
5295.7751	3.1732	0.0069	-0.0048
5296.7550	3.3926	0.0070	-0.0240
5297.8185	3.2263	0.0083	-0.0076
5298.7732	3.1696	0.0073	-0.0303
5300.8114	3.2652	0.0084	-0.0067
5301.8036	3.1611	0.0088	+0.0268
5305.7269	3.3935	0.0071	-0.0239
5306.7188	3.3411	0.0072	-0.0043
5311.8040	3.3486	0.0088	-0.0356
5317.5927	3.3310	0.0101	-0.0144
5323.6579	3.2985	0.0073	-0.0193
5326.6585	3.2569	0.0071	+0.0065
5327.6832	3.4099	0.0133	-0.0278
5362.4677	3.1436	0.0123	+0.0065
5375.5148	3.2806	0.0080	-0.0043
5388.5621	3.4714	0.0092	-0.0490
5410.5201	3.3512	0.0083	-0.0182
5414.4912	3.1813	0.0083	-0.0024

Table 2: Stellar parameters of WASP-41 from spectroscopic analysis.

Parameter	Value
T_{eff} [K]	5450 ± 150
$\log g$	4.4 ± 0.2
ξ_t [km s ⁻¹]	1.0 ± 0.2
$v \sin i$ [km s ⁻¹]	1.6 ± 1.1
[Fe/H]	-0.08 ± 0.09
[Na/H]	0.07 ± 0.09
[Mg/H]	0.07 ± 0.16
[Al/H]	-0.01 ± 0.08
[Si/H]	0.05 ± 0.06
[Ca/H]	0.08 ± 0.15
[Sc/H]	0.01 ± 0.10
[Ti/H]	0.00 ± 0.10
[V/H]	0.06 ± 0.17
[Cr/H]	0.00 ± 0.05
[Mn/H]	0.00 ± 0.13
[Co/H]	-0.01 ± 0.07
[Ni/H]	-0.04 ± 0.06
$\log A(\text{Li})$	< 0.5
Mass [M_{\odot}]	0.95 ± 0.09
Radius [R_{\odot}]	1.01 ± 0.26
Sp. Type	G8 V
Distance [pc]	180 ± 60

Note: Mass and Radius estimate using the Torres et al. (2010) calibration. Spectral Type estimated from T_{eff} using the table in Gray (2008).

lowing definition of the power at angular frequency ω ,

$$P_n(\omega) = \frac{\chi_0^2 - \chi^2(\omega)}{\chi_0^2},$$

where

$$\chi_0^2 = \sum \frac{m_i^2}{\sigma_i^2}$$

and

$$\chi^2(\omega) = \sum \frac{(m_i - y_i)^2}{\sigma_i^2}.$$

We used this definition of the power to search for periodicity in the WASP-South lightcurves of WASP-41 at 4096 evenly spaced frequency values from 0 to 2.5 cycles/day. Variability due to star spots is not expected to be coherent on long timescales as a consequence of the finite lifetime of star-spots and differential rotation in the photosphere so we analysed the two seasons of data

for WASP-41 separately. The signal of the transits in the data was removed using a model similar to the one described below, although in practice this has a negligible effect on the periodogram. We also analysed 3 nearby stars of similar magnitude and colour observed simultaneously with the same camera. The results are shown in Table 3. The periodograms of WASP-41 and one of the nearby stars are shown in Fig. 4.

We used the method of Press and Rybicki (1989) to allow for fast and accurate computation of the periodogram. This enabled us to investigate the significance levels of any peaks in our periodograms using a boot-strap Monte-Carlo approach. We generated synthetic data sets using a method similar to that devised by Collier Cameron et al. (2009), in which data are shuffled according to the date on which the data were obtained. The shuffling procedure shifts each night’s observations in their entirety to a new date. This procedure effectively destroys coherent signals with periods longer than 1 day, but retains the global form of the window function and the effects of correlated noise. In addition to shuffling the date of the observations, we also change the sign of all the data from a given night for a random selection of half of the dates of observation.

Collier Cameron et al. (2009) use a single simulated data set to estimate the parameter N_{eff} in the following model for the distribution of power in the periodogram in the absence of any periodic signal;

$$\text{Prob}(P_n > P'_n) = (1 - P'_n)^{(N_{\text{eff}}-3)/2}.$$

They then use this model to estimate the false alarm probability, FAP, for the highest peak in the periodogram of the actual data from

$$\text{FAP} = 1 - [1 - \text{Prob}(P_n > P'_n)]^M,$$

where $M = (t_N - t_1)(f_{\text{max}} - f_{\text{min}})$ is an estimate of the number of independent frequencies in the periodogram calculated over the range of frequencies f_{min} to f_{max} .⁴ We found from simulations of a large number of data sets using both the “night-shuffling” method and Gaussian random

noise that this method gives inaccurate estimates of FAP, particularly when this value is small. The principle reason for this is that the value of N_{eff} estimated from a single periodogram has a rather large uncertainty, typically around 20% for the data sets we investigated. We found that the following empirical model gives a good representation of the distribution of the peak power $P_{n,\text{best}}$ in the periodograms we generated from simulated data

$$\log_{10}[\text{Prob}(P_{n,\text{best}} > P'_{n,\text{best}})] = c_0 + c_1 P'_{n,\text{best}} + c_2 \left(P'_{n,\text{best}}\right)^2$$

For the analysis of a given set of data we use this model to fit the distribution of peak power values in 1024 simulated data sets. We then use the values of c_0 , c_1 and c_2 to calculate the power corresponding to FAP=0.1, 0.01 and 0.001 shown in Fig. 4 and to estimate the FAP value for the highest peak in the actual periodogram given in Table 3.

There is a clear peak in the periodogram for WASP-41 near $P=18$ d, although there appears to be a difference in the period derived from the two seasons of data (17.6 d and 18.4 d). We inspected the periodograms from the first season of data for WASP-41 and the three nearby stars and found that they all show power near 1 d, 30 d and various combinations of these frequencies and their harmonics, presumably as a result of systematic errors in the photometry related to the diurnal and lunar cycles. In contrast, there is very little spurious power in the periodograms for the second season of data. For this reason we identify the period of 18.41 ± 0.05 d derived from the second season of data as the correct rotation period for WASP-41. We estimated the standard error of the period measurement by analysing 1024 data sets with the same number of points as the original sample, randomly re-sampled with reselection from the original data.

5. Planetary parameters

Our radial velocity (RV) and bisector span (BS) measurements for WASP-41 are shown in Fig. 5 as a function of the photometric transit phase. There is a weak but statistically significant anti-correlation between these RV and BS values. In principle, such an anti-correlation can be used to

⁴Note that there is an error in equation (2) of Collier Cameron et al., the equation for FAP given here is the one actually used in that paper.

Table 3: Period analysis of WASP-42 and nearby stars of similar magnitude and colour.

Star	V	B–V	Year	N	RMS	P_{best}/d	Power	FAP
WASP-41	11.6	0.7	2007	5673	0.041	17.62	0.358	2×10^{-5}
			2008	4966	0.019	18.41	0.240	6×10^{-7}
TYC 7247-1008-1	11.8	0.3	2007	5414	0.026	1.00	0.167	0.07
			2008	4834	0.012	0.98	0.023	0.65
TYC 7247-459-1	11.5	0.5	2007	5389	0.025	96.38	0.101	0.07
			2008	5003	0.012	1.62	0.006	0.45
TYC 7247-683-1	11.2	0.5	2007	5325	0.024	86.23	0.089	0.06
			2008	4993	0.012	0.46	0.005	1.00

identify spurious RV signals caused by stellar activity. For example, (Queloz et al. 2001) showed that the apparent RV signal in HD166435 is caused by stellar activity by identifying 3 characteristics of the signal: i. the RV signal was not coherent over timescales of more than 30 days; ii. the amplitudes of the BS and RV variation were similar; iii. the BS variations were correlated with the photometric variations of the star. In the case of WASP-41 there is no doubt that the RV signal is due to the presence of a planetary mass companion to WASP-41 and not due to stellar activity because: i. the RV signal is coherent over a timescale of more than 200 days; ii. the amplitude of the BS variation is an order of magnitude smaller than the RV variation; iii. the BS values are also correlated with the phase calculated for a rotation period of 18.4d established from the photometric variations of WASP-41. As an additional test of the reality of the planetary RV signal we also re-measured the RV values using a K5-type mask instead of a G2-type mask. Looking for a difference between the RV values derived with the different masks is an effective method for detecting spurious RV signals caused by star spots or faint eclipsing binary stars blended with the target star. In the case of WASP-41 there is no significant difference in the RV values measured with the two masks so the best explanation for the observed RV and BS signals is that WASP-41 has a planetary mass companion with an orbital period of 3.05d.

The CORALIE radial velocity measurements were combined with the WASP-South and FTS photometry in a simultaneous Markov-chain Monte-Carlo (MCMC) analysis to find the parameters of the WASP-41 system. We removed the photometric variation due to stellar rotation from

the WASP-South photometry by subtracting a first-order harmonic series, fit by least-squares to the differential magnitudes from each season independently. The shape of the transit is not well defined in the WASP-South or FTS photometry, so we have imposed an assumed main-sequence mass-radius relation as an additional constraint in our analysis of the data. The stellar mass is determined from the parameters T_{eff} , $\log g$ and $[\text{Fe}/\text{H}]$ using the procedure described by Enoch et al. (2010), based on the compilation of eclipsing binary data by Torres et al. (2010). The code uses T_{eff} and $[\text{Fe}/\text{H}]$ as MCMC jump variables, constrained by Bayesian priors based on the spectroscopically-determined values given in Table 2. Limb-darkening coefficients are taken from Claret (2000).

The parameters derived from our MCMC analysis assuming a circular orbit are listed in Table 4. We found that the contribution to the value of χ^2 for the fit from the RV data was much higher than expected given the standard errors of these measurements. This is a result of additional noise in the RV data due to stellar activity (“jitter”). The free parameters in the fit to the RV are T_0 , P , γ and K , but the values of T_0 and P are determined almost entirely by the photometric data, so the number of degrees of freedom in the fit to the RV data is approximately 20. To achieve a contribution to the value of χ^2 from our 22 RVs of approximately 20 we found that we needed to add 21 ms^{-1} in quadrature to the standard errors for the RV data. We also performed an MCMC analysis of the data including the parameters $\sqrt{e} \cos \omega$ and $\sqrt{e} \sin \omega$ as free parameters. These parameters are used to describe an eccentric orbit solution because they are not strongly correlated and

are equivalent to assuming uniform prior distribution for the value of the eccentricity, e . With this eccentric-orbit solution and the same value of the jitter as the circular orbit solution we find $e = 0.10 \pm 0.06$. As this is consistent with a circular orbit we adopt the parameters from the circular orbit solution. As we do not know *a priori* that the orbit is circular, we take the standard errors on the parameters from the non-circular orbit solution.

We considered the contribution of correlated errors (“red noise”) to the standard errors quoted in Table 4. While the individual transits in the WASP data are affected by red noise, the analysis of the combined lightcurve covering many individual transits will not be strongly affected by red noise because there will be no correlation between the systematic noise from different nights. The FTS lightcurve is affected by red noise so we have investigated the effect of this using the “prayer bead” method. A separate MCMC analysis was performed in which synthetic FTS lightcurves were created from the model fit to the lightcurve and the residuals from this model after cyclic permutation at each step in the MCMC chain. We find that this does not significantly increase the error estimates for any of the parameters.

Another issue to consider for the FTS lightcurve is the effect of starspots on the lightcurve, particularly given the sparse phase coverage of this lightcurve. Star-spots can affect the parameters derived from this lightcurve in two ways. Firstly, the normalization of the lightcurve can be affected by the overall change in brightness of the system due to the 18.4d rotational modulation of the lightcurve. Secondly, small star spots covered by the planet during the transit distort the shape of the lightcurve in a way that may be hard to spot by-eye, but that introduce a systematic error in the parameters derived (Miller-Ricci et al. 2008). We have identified parameters in our solution that are determined primarily by the FTS lightcurve by performing an MCMC solution using the WASP and CORALIE data only. We find that the depth of transit and the planet radius are the only parameters for which the standard error estimates increase significantly in the solution excluding the FTS data. In both cases, the values from the two solutions agree, but the solution

excluding the FTS data has standard error estimates approximately twice as large as the solution including the FTS data. We conclude that these two parameters may be subject to systematic errors comparable to the random errors quoted in Table 4.

We have compared the values of the stellar effective temperature, T_{eff} , and the stellar density, ρ_* to the stellar models of Girardi et al. (2000). We use the parameters T_{eff} and ρ_* because they are independently determined directly from the observations. We find that the mass inferred from the models ($0.9 \pm 0.1M_{\odot}$) is consistent with the mass derived in our MCMC analysis and that the uncertainties on the values of T_{eff} and ρ_* are too large for the models to provide any useful constraint on age of the star. The surface gravity derived from our MCMC solution is consistent with the $\log g$ value from the analysis of the spectrum, but the large uncertainty on the latter value means that this is a rather weak constraint.

6. Discussion

WASP-41 b joins a growing number of planets discovered with masses $\approx 0.9M_{\text{Jup}}$, radii $\approx 1.2R_{\text{Jup}}$ orbiting solar-like stars with periods of about 3 days, e.g., HAT-P-13 b, XO-1 b, WASP-28 b, CoRoT-12 b, WASP-26 b, HAT-P-5 b, HAT-P-6 b, etc.⁵ The WASP-41 planetary system is also similar to the TrES-1 system, particularly in regard to the activity level of the host star.

Knutson et al. (2010) suggest that there is a clear connection between the properties of the emission spectra from hot Jupiters and the activity levels of their host stars. In general, the emission spectrum of hot Jupiters measured from the eclipse depths at infrared wavelengths can only be matched by models that include a high-altitude temperature inversion. Four exceptions to this general rule are the planets orbiting the stars HD 189733, TrES-3, TrES-1 and WASP-4. Knutson et al. found that all four of these stars show moderate levels of chromospheric activity, higher than for all the other stars for which they were able to measure a value $\log R'_{\text{HK}}$. The available evidence supports a hypothesis in which some source of optical opacity high in the atmosphere

⁵<http://exoplanet.eu>

of hot Jupiter planets causes a temperature inversion, but that this opacity source is destroyed by the UV flux associated with chromospheric activity. The result found by Knutson et al. has a high statistical significance but is based on a sample of only 15 stars. The situation is further complicated by the correlation between a planet’s surface gravity and the level of chromospheric activity in its host star claimed by Hartman (2010). The values of $\log R'_{HK}$ and $\log g_p$ we have measured for WASP-41 are consistent with the correlation observed by Hartman. The connection between chromospheric activity and temperature inversions can be confirmed in the case of WASP-41 using observations of the secondary eclipse with the IRAC instrument on the Spitzer Space Telescope at $3.6\mu\text{m}$ and $4.5\mu\text{m}$ (Knutson et al. 2010).

In principle, one can use an age–activity relation established from the average behaviour of many solar-type stars to estimate the age of a star based on the measured $\log R'_{HK}$ value. However, solar-type stars have activity cycles with periods of about a decade during which the value of $\log R'_{HK}$ can vary by 10% or more (Baliunas et al. 1995). This means that an age estimate based on a single measurement of $\log R'_{HK}$ has an unknown systematic error that can be large enough to make the age estimate effectively meaningless. A more useful age estimate can be made in this case based on the observed rotation period of the star, $P_{\text{rot}} = 18.4\text{d}$. The calibration of the “gyrochronological” age given by Barnes (2007) implies an age of 1.8 Gyr for WASP-41 with an error of about 15%. Stars with $T_{\text{eff}}=5300\text{--}5600\text{K}$ are seen to be lithium poor in clusters with ages $> 1\text{Gyr}$ such as NGC752, M67 but the majority of stars in this T_{eff} range in clusters with ages of about 600 Myr such as Praesepe and the Hyades, NGC6633 and Coma Berenices are lithium rich. We conclude that the upper limit to the lithium abundance given in Table 2 is consistent with any age greater than about 600 Myr (Sestito and Randich 2005).

WASP-South is hosted by the South African Astronomical Observatory and we are grateful for their ongoing support and assistance. Funding for WASP comes from consortium universities and from the UK’s Science and Technology Facilities Council. We thank the referee for their careful reading of the manuscript and for comments that

improved the quality of this paper.

REFERENCES

- Baliunas, S. L. et al. 1995, *ApJ*, 438, 269
- Barnes, S. A. 2007, *ApJ*, 669, 1167
- Claret, A. 2000, *A&A*, 363, 1081
- Collier Cameron, A. et al. 2009, *MNRAS*, 400, 451
- Collier Cameron, A. et al. 2007, *MNRAS*, 380, 1230
- Enoch, B., Collier Cameron, A., Parley, N. R., and Hebb, L. 2010, *A&A*, 516, A33
- Gillon, M. et al. 2009, *A&A*, 496, 259
- Girardi, L., Bressan, A., Bertelli, G., and Chiosi, C. 2000, *A&AS*, 141, 371
- Gray, D. F. 2008, *The Observation and Analysis of Stellar Photospheres* (Cambridge University Press)
- Hartman, J. D. 2010, *ApJ*, 717, L138
- Knutson, H. A., Howard, A. W., and Isaacson, H. 2010, *ApJ*, 720, 1569
- Magain, P. 1984, *A&A*, 134, 189
- Miller-Ricci, E. et al. 2008, *ApJ*, 682, 593
- Noyes, R. W., Hartmann, L. W., Baliunas, S. L., Duncan, D. K., and Vaughan, A. H. 1984, *ApJ*, 279, 763
- Pollacco, D. et al. 2008, *MNRAS*, 385, 1576
- Pollacco, D. L. et al. 2006, *PASP*, 118, 1407
- Press, W. H. and Rybicki, G. B. 1989, *ApJ*, 338, 277
- Queloz, D. et al. 2001, *A&A*, 379, 279
- Queloz, D. et al. 2000, *A&A*, 354, 99
- Sestito, P. and Randich, S. 2005, *A&A*, 442, 615
- Stetson, P. B. 1987, *PASP*, 99, 191
- Torres, G., Andersen, J., and Giménez, A. 2010, *A&A Rev.*, 18, 67
- Wilson, D. M. et al. 2008, *ApJ*, 675, L113

Table 4: System parameters for WASP-41. The planet equilibrium temperature is calculated assuming a value for the Bond albedo $A=0$. **N.B.** an assumed main-sequence mass-radius relation is imposed as an additional constraint in this solution so the mass and radius of the star are not independent parameters – see Enoch et al. (2010) for details. Parameter values are taken for the solution assuming $e=0$, standard errors on the parameters are taken from the solution with $\sqrt{e}\cos(\omega)$ and $\sqrt{e}\sin(\omega)$ as free parameters.

Parameter	Symbol	Value	Units
Transit epoch (HJD)	T_0	2455343.463 ± 0.001	days
Orbital period	P	3.052401 ± 0.000004	days
Planet/star area ratio ^a	$(R_p/R_*)^2$	0.0186 ± 0.0004	
Transit duration	t_T	0.108 ± 0.002	days
Impact parameter	b	$0.40^{+0.15}_{-0.11}$	R_*
Stellar reflex velocity	K_1	0.135 ± 0.008	km s^{-1}
Centre-of-mass velocity	γ	3.284 ± 0.009	km s^{-1}
Orbital eccentricity	e	0 (fixed)	
Orbital inclination	i	87.7 ± 0.08	degrees
Stellar density	ρ_*	1.27 ± 0.14	ρ_\odot
Stellar mass	M_*	0.93 ± 0.03	M_\odot
Stellar radius	R_*	0.90 ± 0.05	R_\odot
Orbital semi-major axis	a	0.0402 ± 0.0005	AU
Planet radius ^a	R_p	1.20 ± 0.06	R_J
Planet mass	M_p	0.92 ± 0.06	M_J
Planet surface gravity	$\log g_p$	3.16 ± 0.04	[cgs]
Planet density	ρ_p	0.50 ± 0.08	ρ_J
Planet temperature	T_{eq}	1230 ± 50	K

^a These quantities may have a systematic error comparable to the random error due to the influence of starspots on the FTS lightcurve.

Zechmeister, M. and Kürster, M. 2009, A&A, 496,
577